Physica Scripta. Vol. 48, 559–566, 1993

Data-based Methods for Isoelectronic Prediction of Atomic Lifetimes and Energy Levels*

Lorenzo J. Curtis

Department of Physics and Astronomy, University of Toledo, Toledo, Ohio 43606, U.S.A.

Received April 26, 1993; accepted June 6, 1993

Abstract

The use of data-based semiempirical methods to produce high precision predictions and systematizations along isoelectronic sequences is discussed and applied to several examples. Applications include: studies of trends in the lifetimes of resonance transitions in alkali-like isoelectronic sequences; the combined systematization of spin-allowed and spin-forbidden transition probabilities in alkaline earth-like and inert gas-like isoelectronic sequences; the use of screening and quantum defect parametrizations to predict ionization potentials for the Be sequence.

1. Introduction

The historical development of the field of atomic spectroscopy has proceeded in large part through the empirical exposition and predictive systematization of measured data. Empirical approaches have been necessitated by the high precision achievable in optical measurements, which continually increases due to improved methods and technological advances. Despite similar advances in theoretical methods and in computational technology, there is a continuing tendency for high precision measurements to exceed the capabilities of *ab initio* theoretical methods for complex many-electron systems. Empirical regularities are often exploited for predictive guidance in and conceptual interpretation of experimental measurements, as well as to provide insights into the fundamental nature of the underlying physical interactions. Many of the empirical spectroscopic methods that we use today were developed and widely applied by Professor Bengt Edlén, and generations of atomic spectroscopists have based their research on the methods that he presented in his 1964 Handbuch der Physik article [1].

Several recent reviews [2–4] have described the continuing importance of these methods, which can now be applied to data of unprecedented scope and precision. Now the database is obtained not only by classical spectroscopic methods, but also from light sources utilizing, e.g. magnetically-confined, laser-produced and astrophysically-produced plasmas, or fast ion beam excitation by a foil or laser. Herein we shall restrict the discussion to the systematization of atomic data along isoelectronic sequences, and to illustrate the use of these techniques with a few of our own recent studies.

In describing this work, it is important to differentiate between fully or partially *ab initio* methods and the data-based semiempirical methods which we employ here. *Ab initio* calculations are intended to test fundamental theories and (ideally) proceed directly from first principles, with the only inputs being the wave equation and the fundamental constants. Although *ab initio* calculations are often compromised through empirical corrections (e.g., using experimental wavelengths to convert between absorption and emission rate constants, adjusting configuration amplitudes to yield experimental energies, specifying parameters in a model potential or in perturbative corrections, etc.), the intent remains to produce a wave function that will predict *all* properties of the atom. The data-based empirical formulations presented here have a narrower focus, which is to provide high precision values for one specific quantity over an entire isoelectronic sequence, in a manner that is uniquely specified (by an unambiguous algorithm with no freely adjustable parameters) from measured data. While it might be hoped that the isoelectronic database so produced could also serve as a comprehensive benchmark for the testing of *ab initio* methods, these data-based calculations are not themselves a test of fundamental theory.

Examples will follow which involve: (*i*) the use of transition probability predictions, obtained using wave functions constructed from measured and semiempirically specified spectroscopic energy level data, to investigate small discrepancies between experiment and *ab initio* theory in alkali-like isoelectronic sequences; (*ii*) a systematization of two valence electron and electron–hole spectra that combines energy level and lifetime data, permitting transition probabilities of spin-allowed and spin-forbidden transitions to be treated as equivalent data; and (*iii*) an extension of Professor Edlén's systematization of data for ionization potentials of beryllium-like ions, which yields reliable predictions for the entire isoelectronic sequence.

2. Resonance transition probabilities in alkali-like isoelectronic sequences

Experimental measurements of energy level data have been used to make reliable semiempirical predictions of transition probabilities using the Coulomb Approximation with a Hartree–Slater model core (CAHS) [5–9]. This method involves the integration of the Schrödinger equation with a realistic model potential, constrained to yield the experimental binding energy. The model potential includes the effective central field seen by the single active electron, the spin–orbit interaction, and the core polarization potential

* Dedicated to the memory of Professor Bengt Edlén.

(as specified by the dipole polarizability). The method is formulated to minimize or eliminate the use of adjustable parameters, so that a unique prediction for the transition probability is made entirely from the measured inputs, which are the energy levels, ionization potentials, and core polarizabilities. The applicability of the method can be broadened by the use of other semiempirical studies that interpolate, extrapolate, and smooth these experimental inputs. Recent applications of this method to alkali-like isoelectronic sequences have produced important insights through comparisons to precision experimental measurements and to *ab initio* calculations.

Alkali-like systems, consisting essentially of one electron outside closed shells, have long been assumed to be theoretically calculable with high accuracy. However, small discrepancies between theory [10–17] and experiment [18–30] exist for the $ns\,^2S_{1/2}$–$np\,^2P_{1/2,\,3/2}$ transition probabilities in a number of alkali and alkali-like systems, with *ab initio* calculations consistently shorter in lifetime (by approximately 1%) than experimental measurements. In the 1970s such discrepancies would have been attributed to experimental errors arising from incorrectly treated cascade contributions to curve fit measurements. During the past two decades, such errors have been largely eliminated through the use of cascade-free (e.g., by selective laser excitation) or cascade-compensating (e.g., by correlated analysis of direct cascades (ANDC) [31]) techniques. However, the removal of cascade errors from measured data has reduced but not eliminated these discrepancies, and it now appears possible that the earlier experimental errors were masking a small but significant disagreement between experiment and *ab initio* theory.

There now exists a substantial set of cascade-free lifetime measurements [18–30] made using state-selective laser excitation, which provides lifetimes accurate to 1% or better for a large variety of neutral alkali and singly ionized alkali-like systems. These also include ions such as Ca^+, Sr^+ and Ba^+ for which the lifetime involves a branched decay to ns and $(n-1)d$ levels. A summary of these data is presented in Table I, together with a sampling of *ab initio* calculations [10–17]. Notice that there is a tendency for the *ab initio* calculations to yield lifetimes that are about 1% shorter than the measurements, which are typically of 1% precision. While this trend would not be statistically significant for any single measurement, the systematic trend of the overall sample is unmistakable. Similar 1% discrepancies between experiment and theory have been reported [32] for highly ionized members of the Na isoelectronic sequence.

It should be noted that this comparison is effectively being made among line strengths rather than lifetimes, since experimental wavelength data were used to convert theoretical line strengths to lifetimes. Since theoretical wavelengths tend to be longer than observed for these systems, the use of the corresponding theoretical wavelengths for this conversion would only widen the discrepancies.

Table I also includes a series of semiempirical calculations made using the CAHS algorithm. As can be seen from Table I, these calculations agree very well with experiment, and thus possess the same discrepancies with *ab initio* theory as do the measurements. The CAHS calculations include core polarizability in two different ways: it is contained in the single particle wave functions through the model potential from which they are generated from the energy levels; it is also contained in the electric dipole transition moment,

Table I. *Lifetimes in neutral and singly ionized alkali-like systems*

		τ(ns)			
				Ab initio theory	
Atom	Transition	Experiment	CAHS[a]	MCHF[b,c]	MBPT[d]
Li	$2s_{1/2}$–$2p_{1/2}$	27.20 (20),[e] 27.29 (4)[f]	27.305	27.07	27.04
Na	$3s_{1/2}$–$3p_{1/2}$	16.38 (8),[g] 16.40 (5),[h] 16.40 (3)[f]	16.399	16.12	16.24
	$3s_{1/2}$–$3p_{3/2}$	16.36 (20),[g] 16.35 (5)[h]	16.352	16.07	16.18
Mg^+	$3s_{1/2}$–$3p_{1/2}$	3.854 (30)[i]	3.872	3.86	3.86
	$3s_{1/2}$–$3p_{3/2}$	3.810 (40)[i]	3.842		3.84
Ca^+	$4s_{1/2}$–$4p_{1/2}$	7.07 (7),[j] 7.098 (20)[k]	7.045	6.93	6.94
	$4s_{1/2}$–$4p_{3/2}$	6.87 (6),[j] 6.924 (19)[k]	6.852	6.74	6.75
Cu	$4s_{1/2}$–$4p_{1/2}$	7.27 (6)[l]	7.251	6.87	—
	$4s_{1/2}$–$4p_{3/2}$	7.17 (6)[l]	7.069	6.68	—
Sr^+	$5s_{1/2}$–$5p_{1/2}$	7.47 (7)[m]	—	—	7.48
	$5s_{1/2}$–$5p_{3/2}$	6.69 (7)[m]	—	—	6.74
Ag	$5s_{1/2}$–$5p_{1/2}$	7.408 (32)[n]	7.178	6.29	—
	$5s_{1/2}$–$5p_{3/2}$	6.791 (19)[n]	6.554	5.79	—
Ce	$6s_{1/2}$–$6p_{1/2}$	34.0 (6)[o]	34.961	—	35.22
	$6s_{1/2}$–$6p_{3/2}$	30.55 (27)[p]	30.563	—	30.81
Ba^+	$6s_{1/2}$–$6p_{1/2}$	7.92 (8)[m]	—	—	7.99
	$6s_{1/2}$–$6p_{3/2}$	6.312 (16)[q]	—	—	6.39

[a] C. E. Theodosiou *et al.*: Li Ref. [5]; Na, Mg^+, Ref. [6]; Cu, Ref. [7]; Ca^+, Ref. [8]; Sr^+, Ag, Ce, Ba^+, Ref. [9]. [b] Froese Fischer *et al.*: Li, Na, Ref. [10]; Mg^+, Ref. [11]; Ca^+, Ref. [12]. [c] Carlsson: Cu, Ref. [13]; Ag, Ref. [27]. [d] Johnson *et al.*: Li, Ref. [14]; Na, Mg^+, Ref. [15]; Ca^+, Sr^+, Ba^+, Ref. [16]; Ce, Ref. [17]. [e] Carlsson and Sturesson, Ref. [18]. [f] Gaupp *et al.*, Ref. [19]. [g] Carlsson, Ref. [20]. [h] Schmoranzer *et al.*, Ref. [21]. [i] Ansbacher *et al.*, Ref. [22]; [j] Gosselin *et al.*, Ref. [23]. [k] Jin and Church, Ref. [24]. [l] Carlsson *et al.*, Ref. [25]. [m] Kuske *et al.*, Ref. [26]. [n] Carlsson *et al.*, Ref. [27]. [o] Altman and Kazantsev, Ref. [28]. [p] Tanner *et al.*, Ref. [29]. [q] Andrä, Ref. [30].

given by [33, 34]

$$\boldsymbol{d} = e\boldsymbol{r} - \alpha_d \boldsymbol{r}/r^3, \tag{1}$$

which coherently combines the moments of both the outer electron and the inner core. Tests of the CAHS calculations indicate that the trial exclusion of the core polarizability from the construction of the wave functions has an insignificant effect on the computed lifetimes, but a trial setting of $\alpha_d = 0$ in eq. (1) shortens the computed lifetimes by an amount approximately corresponding to the discrepancy between experiment and *ab initio* theory.

Since the CAHS semiempirical results are essentially uniquely determined from the empirical energy level data (the use of an empirically determined model potential removes the sensitivity to radial cutoffs that is present in standard Coulomb approximation calculations), there are no free parameters to adjust. The semiempirical approach forces the wave functions to yield the correct experimental energies, whereas the *ab initio* wave functions tend to underestimate the experimental binding energies by a few percent. While questions concerning its origin remain, there is no doubt that there exists a small but significant discrepancy between *ab initio* theory and the combined results of experiment and semiempirical prediction for these alkali-like resonance transitions.

Comprehensive compilations of CAHS predictions for entire alkali-like isoelectronic sequences are now available [5–9]. Experimental measurements which test these predictions for selected cases at very high stages of ionization would be very useful in resolving the questions discussed above. If the reliability exhibited by the CAHS computations persists to high Z, this would indicate that wave functions that accurately predict transition wavelengths also accurately predict the line strengths.

3. Intermediate coupling formulations which utilize energy level data to combine transition probabilities of spin-allowed and spin-forbidden decays

In studies of ns^2–$nsn'p$ and np^6–$np^5n's$ transitions in alkaline-earth-like and inert gas-like isoelectronic sequences, an empirical data reduction has been developed [35–40] that treats measured transition probabilities for the resonance and intercombination lines as conjugate quantities. The reduction is formulated through a singlet–triplet mixing angle θ that is deduced from measured spectroscopic energy level data, and yields effective generalized line strengths that have a regular and slowly varying isoelectronic behaviour. This regularity has been observed to persist even in the presence of strong perturbations, and it can be linearized through a simple screening parametrization that permits quantitative interpolation, extrapolation and smoothing.

This semiempirical data reduction method consists of: specification of an effective single configuration singlet–triplet mixing angle θ from experimental energy level data; the use of θ and experimental wavelength data to construct reduced line strengths S_r from experimental transition probability data for the resonance and intercombination lines; and the exposition and parametrization of S_r.

For a pure $nsn'p$ or $np^5n's$ configuration, the singlet and triplet $J = 1$ states can be written in terms of a mixing angle θ as

$$|{}^3P_1'\rangle = \cos\theta\,|{}^3P_1\rangle - \sin\theta\,|{}^1P_1\rangle$$
$$|{}^1P_1'\rangle = \sin\theta\,|{}^3P_1\rangle + \cos\theta\,|{}^1P_1\rangle, \tag{2}$$

where the primes indicate the mixed states, for which the LS labels are only nominal. If the measured excitation energies of the ${}^3P_0$, ${}^3P_1'$, ${}^3P_2$ and ${}^1P_1'$ levels are denoted by E_{30}, E_{31}, E_{32} and E_{11}, θ can be deduced from the data using [35]

$$\cot(2\theta) = \pm\frac{1}{\sqrt{2}}\left[\frac{3(E_{31} + E_{11} - 2E_{30})}{2(E_{32} - E_{30})} - 1\right]. \tag{3}$$

This mixing angle also relates the radial dipole transition integrals to the line strengths for ns^2–$nsn'p$ or np^6–$np^5n's$ resonance and intercombination transitions S(Res) and S(Int), which are given by

$$S(\text{Res}) = 2\cos^2\theta\,|\langle ns_0\,|\,r\,|\,n'p_0\rangle|^2$$
$$S(\text{Int}) = 2\sin^2\theta\,|\langle ns_0\,|\,r\,|\,n'p_1\rangle|^2. \tag{4}$$

(with radial wave functions $|n\ell_S\rangle$). Measured transition probabilities A for a $J = 1$ level can be converted to line strengths by the relationship

$$S = 3[\lambda(\text{Å})/1265.38]^3 A\,(\text{ns}^{-1}), \tag{5}$$

where λ is the transition wavelength. The reduced line strengths (which involve only radial matrix elements) are then defined from eq. (4) as

$$S_r(\text{Res}) \equiv S(\text{Res})/\cos^2\theta$$
$$S_r(\text{Int}) \equiv S(\text{Int})/\sin^2\theta. \tag{6}$$

The empirical quantities are often accurately represented by a screening parameter linearization

$$Z^2 S_r \cong a + b/(Z - c). \tag{7}$$

In general there are separate values of a and b for the data from the resonance and intercombination transitions, but there are cases where the two parametrizations coincide.

If the singlet–triplet splitting is small and the transition integrals do not have strong cancellation effects, it can happen that $\langle ns_0\,|\,r\,|\,n'p_0\rangle \cong \langle ns_0\,|\,r\,|\,n'p_1\rangle$. In such cases S_r(Res) and S_r(Int) are equivalent measures of a single quantity S(Tot), which is the total line strength for the $J = 0$–1 transition,

$$S(\text{Tot}) \equiv S(\text{Res}) + S(\text{Int}) = S(\text{Res})/\cos^2\theta$$
$$= S(\text{Int})/\sin^2\theta. \tag{8}$$

In cases where $S(\text{Tot}) = S_r(\text{Res}) = S_r(\text{Int})$, measurements of the resonance and intercombination transition probabilities follow the same linear relationship in eq. (7). This can be particularly useful since the combined use of resonance and intercombination transitions to specify a generalized line strength permits data over a wide range of charge states to be merged. Time-of-flight methods are limited to lifetimes that produce a measurable decay length, and often the intercombination transitions are immeasurably long-lived at low Z and the resonance transitions are immeasurably short-lived at high Z. In these cases lifetime measurements for the resonance transition can be used to predict lifetimes for the intercombination transitions and vice versa.

Although this analysis is based on a single configuration picture, the parametric angle θ can be used to uniquely characterize the data irrespective of the presence of configuration interaction. Empirical evidence indicates that the

influence of configuration interaction is often indirect: it alters the singlet–triplet mixing but not the transition integrals. Thus, even in the presence of plunging configuration interaction, the isoelectronic irregularities in the transition probabilities are accompanied by irregularities in the energy level structure, but these compensate to yield a smooth data exposition in terms of S_r.

This approach has been applied to the unbranched intrashell resonance and intercombination lines for the ns^2–$nsnp$ transitions in the Be ($n = 2$), Mg ($n = 3$), and Zn ($n = 4$) isoelectronic sequences [37, 39]. The Zn sequence is particularly noteworthy, since a recent restudy [40] of its intercombination transition probabilities revealed errors in both the calculations and measurements, and this had caused deceptive agreement. Hibbert and Bailie [41] recently showed that earlier theoretical calculations had overestimated these lifetimes because of a failure to include the effects of core polarization, and suggested a procedure for correcting these predictions. Träbert and coworkers [42, 43] have subsequently made new lifetime measurements of these intercombination transitions for several ions, and demonstrated that the earlier measurements had overestimated the lifetimes because of a failure to adequately account for the effects of cascade repopulation. (A faulty experimental assumption had been made that, because these spin-forbidden transitions are longer-lived than their close-lying cascade feeders, their repopulation would be less significant than in spin-allowed cases.) As will be shown below, the correction of these errors has interesting implications when examined within the mixing angle formulation.

An earlier mixing angle reduction [39] of the lifetime data then available had indicated that the values of S_r(Res) and S_r(Int) were both linear in $1/(Z - 28)$, but that each had its own characteristic slope and intercept, as represented by eq. (7). When the revised data for the intercombination lifetimes were included and subjected to this same reduction, a shift occurred which moved the S_r(Int) values onto the same straight line as S_r(Res). Figure 1 displays a plot of these values, with the resonance transition denoted by (X) and the intercombination transitions denoted by (0). A fit to the combined data is indicated by the solid line. Figure 1 demonstrates that, for the $4s^2$–$4s4p$ transitions in the Zn sequences, S_r(Res) and S_r(Int) are equivalent measures of S(Tot) as defined in eqs (6)–(8).

The mixing angle reduction method has also been applied to the $2s^2$–$2s3p$ transition in the Be isoelectronic sequence [38]. This extension to a branched intershell transition provides a stringent test for the method, since it introduces complications from plunging configuration interaction, transition integral cancellations and multiple exit channels that were not present for the intrashell transitions. However, this requires the experimental specification of the transition probability of the intercombination channel of a branched decay, a quantity not usually obtained from lifetime measurements. In this case measurements do exist, because a novel experimental technique [44] permits the determination of intercombination transition probabilities through differential decay curve measurements that exploit the J dependence of the exit channels of the triplet levels.

Using measurements for N IV, O V, F VI [44] and Ne VII [45], a linearizing mixing angle formulation of the intercombination transition was obtained that also predicts

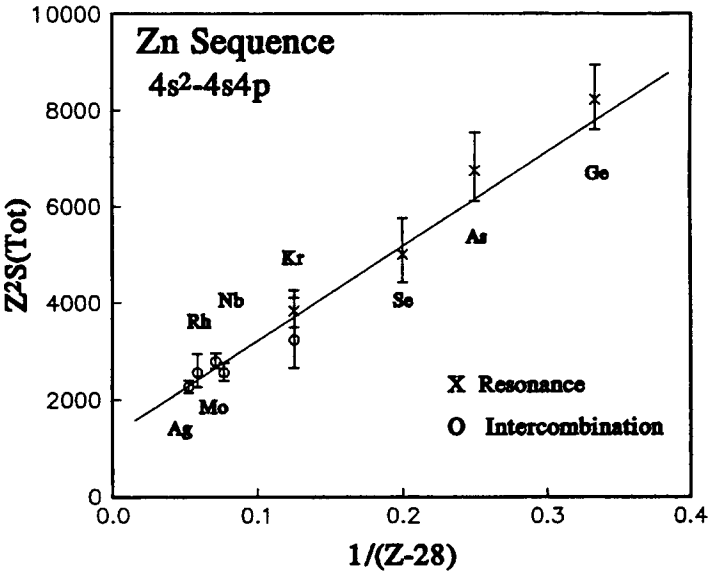

Fig. 1. Isoelectronic plot of the total charge-scaled line strength of the $4s^2$–$4s4p$ ($J = 0$–1) transitions in the Zn isoelectronic sequence *vs.* the effective reciprocal core charge. Values for Z^2S_r(Res) deduced from the singlet–singlet resonance transition are denoted by (X); values for Z^2S_r(Int) deduced from the singlet–triplet intercombination transition are denoted by (0). The solid line denotes a linear fit to the combined resonance and intercombination transition data.

the lifetime of the resonance transition with high reliability. Here again, to within experimental uncertainties, S_r(Res) and S_r(Int) were found to lie along the same fitted line when plotted *vs.* $1/(Z - 3)$, thus simultaneously determining S(Tot), as defined in eqs (6)–(8). Recent measurements [46] have confirmed that these trends also hold for the $2s^2$–$2s3p$ intercombination transitions in Be-like Na, Mg, Al and Si.

The lifetimes of the $2p^6$–$2p^53s$ transitions in the Ne isoelectronic sequence have also been studied by the mixing angle reduction approach. These transitions are particularly interesting because it is possible to create a population inversion between the $2p^53s$ and $2p^53p$ levels that can produce XUV laser amplification action. Modelling studies have demonstrated that amplification is optimal near $Z = 36$, leading to tests in Se [47] and Y [48] plasmas. Although the lifetimes of these levels are too short for time-of-flight measurements at $Z = 36$, the mixing angle formulation permits semiempirical extrapolation if precise results at lower Z are available.

We recently performed precision measurements of these lifetimes in transitions in S VII and Cl VIII [49]. These studies were made possible by the existence of a uniquely designed beam-foil chamber at the University of Lund, which views a very short segment of beam with a grazing incidence monochromator, permitting the precision measurement of lifetimes as short as a few ps for wavelengths well below 100 Å. These measurements yielded lifetimes accurate to 3–4%, as compared to earlier measurements for these ions [50, 51] which had uncertainties $\geqslant 25\%$. In addition to the curve fits, it was also possible to perform ANDC correlated analyses, including the decay curves of both the primary $2p^6$–$2p^53s$ transitions and the dominant $2p^53s$–$2p^53p$ cascade repopulation channel (which is a proposed laser transition).

Figure 2 presents a reduction of selected experimental data to values for S_r(Res) and S_r(Int) plotted *vs.* $1/(Z - 9)$. This includes our values for S VII and Cl VIII data [49] as

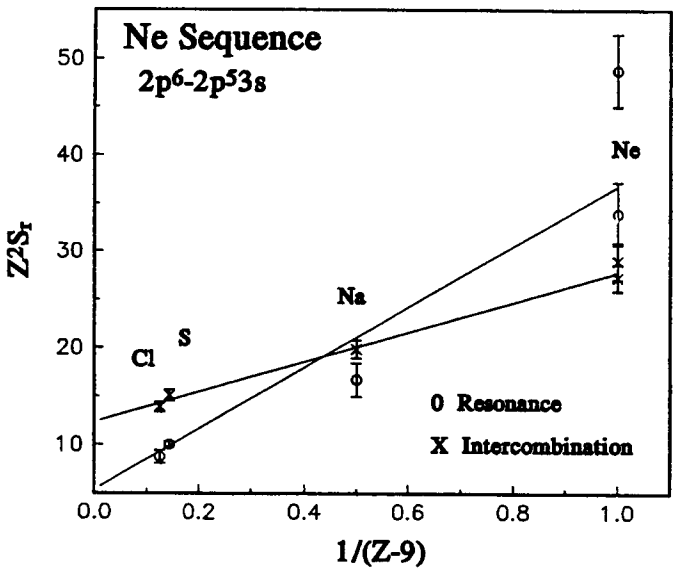

Fig. 2. Isoelectronic plot of the charge-scaled reduced line strengths of the $2p^6$–$2p^5 3s$ ($J = 0$–1) transitions in the Ne isoelectronic sequence *vs.* the effective reciprocal core charge. Values for Z^2S_r(Res) deduced from the singlet–singlet resonance transition are denoted by (0); values for Z^2S_r(Int) deduced from the singlet–triplet intercombination transition are denoted by (X). The solid lines indicate two separate linear fits: one to the resonance transition data; another to the intercombination transition data.

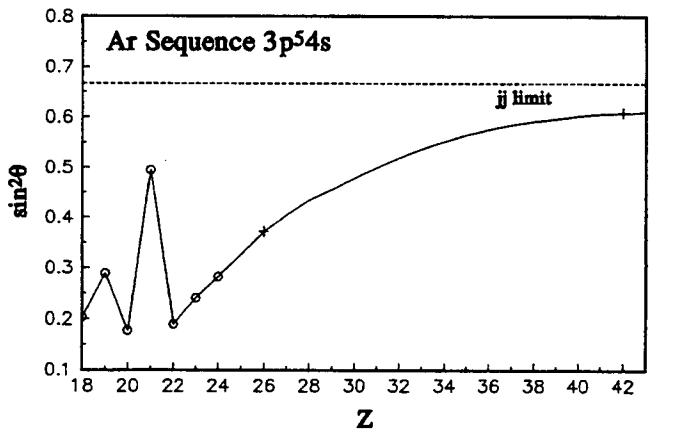

Fig. 3. Isoelectronic plot of the squared sine of the singlet–triplet mixing angle for the $3p^5 4s$ ($J = 1$) levels in the Ar sequence *vs.* the isoelectronic nuclear charge. The values were obtained by applying eq. (3) to data in Refs [49, 52–54].

well as the available data for Ne I [52, 53] and Na II [54]. Earlier measurements [50, 51] for S VII, Cl VIII and Ar IX were omitted because they are of lower precision, and confuse the plot with scattering about the recent results without altering a weighted fit to the data. The error bars denote the quoted uncertainties for all cases except the Na II resonance transition, where the quoted error [54] was unrealistic (0.5%) and was increased by a factor of ten. For this sequence it was necessary to make separate fits to eq. (7) for the resonance and intercombination transitions, which are indicated by the solid lines. For the intercombination transitions the measurements are of uniformly high precision, and the data points lie along the same straight line on this plot. For the resonance transitions the Ne I and Na II measurements are of lower accuracy (the two measurements for Ne I differ significantly) and there is scatter about the line.

If the linear fit exhibited in Fig. 2 is extrapolated to Se ($Z = 34$) it implies lifetimes for the resonance and intercombination lines of 0.43 and 0.13 ps (the reversed ordering occurs because of the avoided crossing at $Z \cong 21$). While measurements here do not include a sufficiently broad sample of ions to test the validity of the linear relationship, existing *ab initio* calculations vary by factors of 2. If this semiempirical approach proves to be extrapolatively reliable to a degree commensurate with the 3–4% accuracies provided by our measurements, these estimates would be valuable for plasma modelling purposes.

A similar analysis has been made of data for the $3p^6$–$3p^5 4s$ transitions in the Ar isoelectronic sequence. Spectroscopic energy level data [55, 56] for $3p^5 4s$ were reduced to effective single configuration mixing angles using eq. (3) and $\sin^2\theta$ is plotted *vs.* the nuclear charge Z in Fig. 3. This analysis suggests that experimental studies in the vicinity of Sc IV would be particularly interesting, because in this ion the plunging $3p^5 3d\,{}^1P_1$ level causes a strong local enhancement (50% as shown in Fig. 3) in the effective single configuration singlet–triplet mixing. Studies using theoretical values [56] for the line strengths indicate that, while both the energy levels and the lifetime are strongly perturbed in the vicinity of the level crossing, the values for S(Tot) are isoelectronically smooth. Here lifetime measurements would test the validity of the assumption that configuration interaction is indirect, perturbing the lifetimes and the energy levels (and hence the mixing angle), but not the transition matrix.

4. Ionization potentials for the Be isoelectronic sequence

Spectroscopically, ionization potentials (IP) are determined by two alternative approaches [57]: the quantum defect method and the core polarization model. In the quantum defect method, transition wavelengths between two interacting low ℓ Rydberg series are first mapped onto effective quantum numbers by the Balmer formula, then parametrized by a Ritz expansion, and finally extrapolated to $n \Rightarrow \infty$. In the core polarization model, transition wavelengths between n and ℓ states are represented by a single hydrogenic electron moving in the field of the nucleus and a deformable cloud of core electrons. The two methods are complementary, and in some cases both approaches have been applied to the same system with good agreement. However, for reliable results, either method requires that the observations and the analysis of the spectrum be quite comprehensive. To extend these results to high degrees of ionization where only fragmentary spectroscopic classification work is available, semiempirical extrapolations must be made.

The Be isoelectronic sequence provides an excellent candidate for semiempirical extrapolation. Here experimental data are available only for Be I–Si XI [58–65] and for Fe XXIII [55], and for other ions only the extrapolations through Cu XXVI by Lotz [66] and theoretical estimates are available. Edlén [57] suggested an extrapolation procedure that separates the parametrization into two parts, representative of the internal and external portions of the wave function. The internal portion characterizes the Sommerfeld fine structure and the quantum electrodynamic (QED) corrections, which sample the wave function weighted by $1/r^3$, and are represented by a very weakly

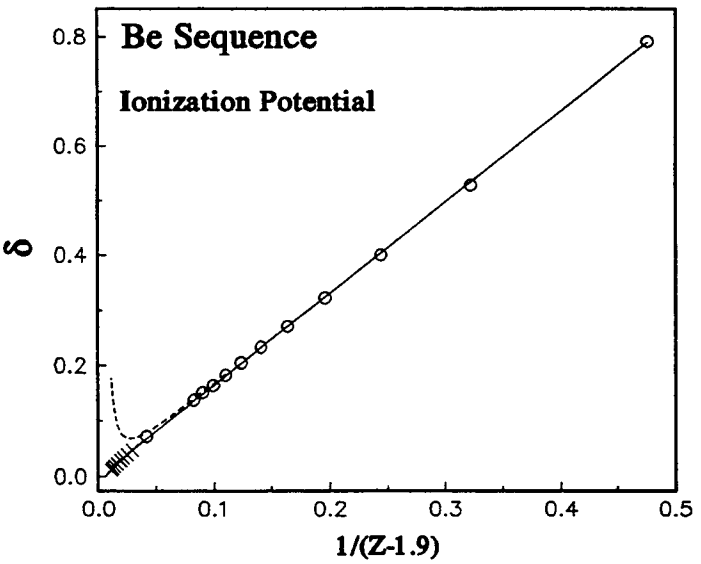

Fig. 4. Isoelectronic plot of the quantum defect *vs.* the effective reciprocal core charge for the ionization potentials in the Be sequence. The experimental data are noted by (0), MCDF calculations are denoted by (X), and the solid line denotes a linear fit to the experimental data. The dashed line indicates the locus that the experimental and MCDF quantum defects follow when the fine structure and QED corrections are not stripped off before their computation.

screened hydrogen-like formula. The external portion characterizes the Balmer energy, which samples the wave function weighted by $1/r$, and is represented by a fully screened hydrogen-like formula.

Following the approach of Edlén [57], we have adopted a mapping model that is constructed of three parts: a fully screened Balmer energy parametrized by a quantum defect; a weakly screened Sommerfeld relativistic energy; and a weakly screened QED energy. For the Sommerfeld and QED energies, hydrogen-like formulae were used with integer quantum numbers and an effective screening of one electron charge. The available data were first reduced by subtraction of the Sommerfeld and QED energies, then mapped into the effective quantum defect, which is then linearly fitted to an effective reciprocal screened charge.

Thus we express the binding energy E_∞ of one of the $2s$ electrons in a Be-like atom as

$$E_\infty = E_B + E_{\rm fs} + E_{\rm qed}, \tag{9}$$

where E_B is the fully screened Balmer energy, written in terms of the quantum defect δ as

$$E_B = R(Z-3)^2/(2-\delta)^2. \tag{10}$$

$E_{\rm fs}$ is the Sommerfeld fine structure energy, and $E_{\rm qed}$ includes the various QED self-energy and vacuum polarization corrections. The higher order corrections to the Balmer energy can be written in terms of a screened charge multi-

Table II. *Semiempirical ionization potentials for the Be sequence*

Z Ion	IP (cm^{-1})	Z Ion	IP (cm^{-1})	Z Ion	IP (cm^{-1})
4 Be	75 193[a]	34 Se	28 296 600	64 Gd	112 816 800
5 B	202 887[b]	35 Br	30 139 800	65 Tb	116 795 900
6 C	386 241[b]	36 Kr	32 044 600	66 Dy	120 860 800
7 N	624 865[c]	37 Rb	34 011 500	67 Ho	125 013 000
8 O	918 657[d]	38 Sr	36 041 000	68 Er	129 253 800
9 F	1 267 606[e]	39 Y	38 133 600	69 Tm	133 584 700
10 Ne	1 671 792[f]	40 Zr	40 289 800	70 Yb	138 007 200
11 Na	2 131 300[g]	41 Nb	42 510 000	71 Lu	142 522 900
12 Mg	2 644 700[g]	42 Mo	44 794 900	72 Hf	147 133 600
13 Al	3 221 080[g]	43 Tc	47 145 000	73 Ta	151 840 800
14 Si	3 842 100[g]	44 Ru	49 560 900	74 W	156 646 400
15 P	4 521 163	45 Rh	52 043 200	75 Re	161 552 200
16 S	5 257 749	46 Pd	54 592 500	76 Os	166 560 300
17 Cl	6 050 253	47 Ag	57 209 500	77 Ir	171 672 600
18 Ar	6 898 839	48 Cd	59 894 800	78 Pt	176 891 300
19 K	7 803 675	49 In	62 649 200	79 Au	182 218 500
20 Ca	8 764 939	50 Sn	65 473 400	80 Hg	187 656 600
21 Sc	9 782 824	51 Sb	68 368 100	81 Tl	193 208 000
22 Ti	10 857 531	52 Te	71 334 100	82 Pb	198 875 300
23 V	11 989 248	53 I	74 372 300	83 Bi	204 661 000
24 Cr	13 178 272	54 Xe	77 483 400	84 Po	210 567 900
25 Mn	14 424 763	55 Cs	80 668 400	85 At	216 599 100
26 Fe	15 797 000[h]	56 Ba	83 928 100	86 Rn	222 757 400
27 Co	17 091 200	57 La	87 263 500	87 Fr	229 046 100
28 Ni	18 511 700	58 Ce	90 675 600	88 Ra	235 468 500
29 Cu	19 990 800	59 Pr	94 165 300	89 Ac	242 028 200
30 Zn	21 532 300	60 Nd	97 733 700	90 Th	248 728 900
31 Ga	23 132 900	61 Pm	101 381 900	91 Pa	255 574 400
32 Ge	24 793 600	62 Sm	105 111 100	92 U	262 569 000
33 As	26 514 700	63 Eu	108 922 300		

[a] Seaton, Ref. [59]. [b] Ölme, Ref. [60]. [c] Hallin, Ref. [62]. [d] Bockasten and Johansson, Ref. [63]. [e] Engström, Ref [64]. [f] Edlén, Ref. [57]. [g] Martin and Zalubas, Ref. [65]. [h] Corliss and Sugar [55].

plied by the fine structure constant α,

$$X \equiv \alpha(Z - S_0). \tag{11}$$

It has been shown [5] that for the Li isoelectronic sequence this screening constant is given approximately by $S_0 = 1$, and that value was adopted to characterize the Sommerfeld and QED fine structure herein. In a formulation presented in Ref. [67], it is shown that E_{fs} can be written as

$$E_{fs} = \frac{R}{\alpha^2} \sum_{p=2}^{\infty} B_p X^{2p} \tag{12}$$

where the coefficients B_p for terms up to $p = 9$ for a $2s$ electron can be obtained from a tabulation [67] as $B_2 = 0.078125$, $B_3 = 0.041016$, $B_4 = 0.026184$, $B_5 = 0.018574$, $B_6 = 0.014016$, $B_7 = 0.011070$, $B_8 = 0.009029$, $B_9 = 0.007546$. It is shown in Ref. [68] that, for a $2s$ electron, the QED corrections can be written

$$E_{qed} = \frac{RX^4}{4\alpha\pi}\left(-\frac{8}{3}\ln X - 2.9053X - (4\ln^2 X - 11.594 \ln X + 25.442)X^2 + 0.1820 + 23.44X^3\right). \tag{13}$$

The fine structure and QED corrections were first subtracted from the experimental values [58–65] for the ionization potential, and the residues were then converted to values for the quantum defect δ. The remaining deviations from the hydrogenic Balmer energy (penetration, polarization and other correlations, etc.) thus reside in the empirical value for δ, and the goal of the parametrization is to obtain a reliable isoelectronic extrapolation of δ. Such a parametrization was obtained using the relationship

$$\delta \cong a + b/(Z - S_1). \tag{14}$$

The results are displayed in Fig. 4. The empirical quantum defects are denoted by (0) and are very well represented by eq. (14). The solid line denotes a least squares adjustment to the values $a = -0.0016$, $b = 1.6613$ and $S_1 = 1.9$. In order to test the high Z extrapolations, we performed multiconfiguration Dirac–Fock (MCDF) calculations [69] of the IP for the selected ions in the range $36 \leqslant Z \leqslant 92$. The MCDF results were reduced by the same procedure (but not included in the fit), and are denoted by (X) in Fig. 4. To investigate the importance of the subtraction of the fine structure and QED corrections, the combined experimental and MCDF data were also reduced to quantum defects without first removing the Sommerfeld and QED energies, which is indicated by a dashed line. The predictions of this semiempirical formulation are presented in Table II.

5. Concluding remarks

The three examples presented here illustrate a wide range of approaches to the utilization of measured data for predictive purposes. The CAHS method uses measured data for one type of quantity to make unique predictions for another type of quantity. The predictions are either verified or refuted by subsequent measurements. The mixing angle formulation permits data for three types of quantities to be combined to make interpolative and extrapolative predictions. Through subsequent measurements the systematizing relationships among these quantities can be verified and the accuracy of the predictions can be enhanced. The ionization potential formulation is a simple linearizing mapping of a quantity into a space where it is regular and slowly varying.

Acknowledgements

I would like to acknowledge the inspiration, encouragement, and friendship that I have received for many years from Bengt and Friedel Edlén. This work was partially supported by the US Department of Energy, Fundamental Interactions Branch, Office of Basic Energy Sciences, Divison of Chemical Sciences, under grant number DE-FG05-88ER13958.

References

1. Edlén, B., in: "Handbuch der Physik", Vol. 27 (Edited by S. Flügge) (Springer-Verlag, Berlin 1964), p. 80.
2. Curtis, L. J., Nucl. Instr. Meth. **202**, 333 (1981); **B31**, 146 (1988).
3. Curtis, L. J., Comments At. Mol. Phys. **16**, 1 (1985).
4. Curtis, L. J., Physica Scripta **35**, 805 (1987); **39**, 447 (1989).
5. Theodosiou, C. E., Curtis, L. J. and El-Mekki, M., Phys. Rev. **A44**, 7144 (1991).
6. Theodosiou, C. E. and Curtis, L. J., Phys. Rev. **A38**, 4435 (1988).
7. Curtis, L. J. and Theodosiou, C. E., Phys. Rev. **A39**, 605 (1989).
8. Theodosiou, C. E., Phys. Rev. **A39**, 4880 (1989).
9. Theodosiou, C. E., personal communication.
10. Froese Fischer, C., Nucl. Instr. Meth. **B31**, 265 (1988).
11. Froese Fischer, C., Can. J. Phys. **54**, 1465 (1976).
12. Vaeck, N., Godefroid, M. and Froese Fischer, C., Phys. Rev. **A46**, 3704 (1992).
13. Carlsson, J., Phys. Rev. **A38**, 1702 (1988).
14. Johnson, W. R., Idrees, M. and Sapirstein, J., Phys. Rev. **35**, 3218 (1987).
15. Guet, C., Blundell, S. A. and Johnson, W. R., Phys. Lett. **A143**, 384 (1990).
16. Guet, C. and Johnson, W. R., Phys. Rev. **A44**, 1531 (1991).
17. Blundell, S. A., Johnson, W. R. and Sapirstein, J. A., Phys. Rev. **A43**, 3407 (1991).
18. Carlsson, J. and Sturesson, L., Z. Physik **D14**, 281 (1989).
19. Gaupp, A., Kuske, P. and Andrä, H. J., Phys. Rev. **A26**, 3351 (1982).
20. Carlsson, J., Z. Physik, **D9**, 147 (1988).
21. Schmoranzer, H., Schulze-Hagenest, D. and Kandela, S. A., Symposium on Atomic Spectroscopy (SAS-79), Tucson, AZ, 1979, Abstracts p. 195.
22. Ansbacher, W., Li, Y. and Pinnington, E. H., Phys. Lett. **A139**, 165 (1989).
23. Gosselin, R. N., Pinnington, E. H. and Ansbacher, W., Nucl. Instr. Meth. Phys. Res. **B31**, 305 (1988).
24. Jin, J. and Church, D. A., Phys. Rev. Lett., **70**, 3213 (1993).
25. Carlsson, J., Sturesson, L. and Svanberg, S., Z. Physik **D11**, 287 (1989).
26. Kuske, P., Kirchner, N., Wittmann, W., Andrä, H. J. and Kaiser, D., Phys. Lett. **A64**, 377 (1978).
27. Carlsson, J., Jönsson, P. and Sturesson, L., Z. Phys. **D16**, 87 (1990).
28. Altman, E. L. and Kazantsev, S. A., Opt. Spekstr. **28**, 805 (1970).
29. Tanner, C. E., Livingston, A. E., Rafac, R. J., Serpa, F. G., Kukla, K. W., Berry, H. G., Young, L. and Kurtz, C. A., Phys. Rev. Lett. **69**, 2765 (1992).
30. Andrä, H. J., in: "Beam-foil Spectroscopy" (Edited by I. A. Sellin and D. J. Pegg) (Plenum, New York 1976), vol. 2, p. 835.
31. Curtis, L. J., Berry, H. G. and Bromander, J., Phys. Lett. **A34**, 169 (1971).
32. Hutton, R., Engström, L. and Träbert, E., Phys. Rev. Lett. **60**, 2469 (1988).
33. Bersuker, I. B., Opt. Spektr. **3**, 97 (1957).
34. Hameed, S., Herzenberg, A. and James, M. G., J. Phys. **B1**, 822 (1968).
35. Curtis, L. J., Phys. Rev. **A40**, 6958 (1989).
36. Curtis, L. J., J. Phys. **B22**, L267 (1989).
37. Curtis, L. J., Physica Scripta **43**, 137 (1991).
38. Curtis, L. J., J. Phys. **B25**, 1427 (1992).
39. Curtis, L. J., J. Opt. Soc. Am. **B9**, 5 (1992).

40. Träbert, E. and Curtis, L. J., Physica Scripta (in press).
41. Hibbert, A. and Bailie, A. C., Physica Scripta **45**, 565 (1992).
42. Träbert, E. and Pinnington, E. H., Can. J. Phys. (in press).
43. Träbert, E., Heckmann, P. H., Doerfert, J. and Granzow, J., Physica Scripta **47**, 780 (1993).
44. Engström, L., Denne, B., Huldt, S., Ekberg, J. O., Curtis, L. J., Veje, E. and Martinson, I., Physica Scripta **20**, 88 (1979).
45. Hardis, J. E., Curtis, L. J., Ramanujam, P. S., Livingston, A. E. and Brooks, R. L., Phys. Rev. **A27**, 257 (1983).
46. Granzow, J., personal communication.
47. Rosen, M. D., Hagelstein, P. L., Matthews, D. L., Campbell, E. M., Hazi, A. U., Whitten, B. L., MacGowan, B., Turner, R. E., Lee, R. W., Charatis, G., Busch, G. E., Shepard, C. L. and Rockett, P. D., Phys. Rev. Lett. **54**, 106 (1985).
48. Matthews, D. L., Hagelstein, P. L., Rosen, M. D., Eckart, M. J., Ceglio, N. M., Hazi, A. U., Medecki, H., MacGowan, B. J., Trebes, J. E., Whitten, B. L., Campbell, E. M., Hatcher, C. W., Hawryluk, A. M., Kauffman, R. L., Pleasance, L. D., Rambach, G. Scofield, J. H., Stone, G. and Weaver, T. A., Phys. Rev. Lett. **54**, 110 (1985).
49. Westerlind, M., Engström, L., Bengtsson, P. and Curtis, L. J., Phys. Rev. **A45**, 6198 (1992).
50. Gardner, R. K., Cocke, C. L., Saylor, T. K. and Curnutte, B., J. Opt. Soc. Am. **68**, 830 (1978).
51. Berry, H. G., Désesquelles, J., Cheng, K. T. and Schectman, R. M., Phys. Rev. **A18**, 546 (1978).
52. Lawrence, G. M. and Liszt, H. S., Phys. Rev. **178**, 122 (1969).
53. Kernahan, J. A., Denis, A. and Drouin, R., Physica Scripta **4**, 49 (1971).
54. Schlagheck, W., Phys. Lett. **A54**, 181 (1975).
55. Corliss, C. and Sugar, J., J. Phys. Chem. Ref. Data **8**, 1109 (1979); **8**, 865 (1979); **9**, 473 (1980); **8**, 1 (1979); **7**, 1191 (1978); **6**, 317 (1977); **6**, 1253 (1977); **11**, 135 (1982).
56. Lin, D. L., Fielder, W. and Armstrong, L., Phys. Rev. **16**, 589 (1977).
57. Edlén, B., in: "Topics in Modern Physics – A Tribute to E. U. Condon" (Edited by W. E. Brittin and H. Odabasi) (Colorado Associated University Press, Boulder 1971), p. 133.
58. Johansson, L., Arkiv Fysik **23**, 119 (1962).
59. Seaton, M. J., J. Phys. **B9**, 3001 (1976).
60. Ölme, A., Physica Scripta **1**, 256 (1970).
61. Bockasten, K., Arkiv Fysik **9**, 457 (1955).
62. Hallin, R., Arkiv Fysik **32**, 201 (1966).
63. Bockasten, K. and Johansson, K. B., Arkiv Fysik **38**, 563 (1968).
64. Engström, L., Physica Scripta **31**, 379 (1985).
65. Martin, W. C. and Zalubas, R., J. Phys. Chem. Ref. Data **8**, 817 (1979); **9**, 1 (1980); **10**, 153 (1981); **12**, 323 (1983).
66. Lotz, W., J. Opt. Soc. Am. **57**, 873 (1967).
67. Curtis, L. J., J. Phys. **B10**, L641 (1977).
68. Curtis, L. J., J. Phys. **B18**, L651 (1985).
69. Grant, I. P., McKenzie, B. J., Norrington, P. H., Mayers, D. F. and Pyper, N. C., Comput. Phys. Commun. **21**, 207 (1980); Dyall, K. G., Grant, I. P., Johnson, C. T., Parpia, F. A. and Plummer, E. P., Comput. Phys. Commun. **55**, 425 (1989).